Adsorption of pure CO_2 and a CO_2/CH_4 mixture on a black shale sample: Manometry and microcalorimetry measurements

Olga Patricia Ortiz Cancino [a,*], David Pino Pérez [b], Manuel Pozo [c], David Bessieres [b]

[a] Universidad Industrial de Santander- GMPH, Bucaramanga, Colombia
[b] Université de Pau et des Pays de l'Adour, UMR 5150, LFC-R- Laboratoire des Fluides Complexes et leurs Réservoirs, 64013 Pau Cedex, France
[c] Department of Geology and Geochemistry, Universidad Autónoma de Madrid, Cantoblanco 28049 Madrid, Spain

ABSTRACT

The study of CO_2/CH_4 adsorption onto kerogen is relevant for shale gas production. Despite much expanded literature, reliable adsorption models still await for a complete description due to the complexity of kerogen. The objective of this study is to provide an original set of experimental data and to use the selectivity as an indicator to test the affinity of the sample for a component over another. The adsorption of pure CO_2 and the equimolar mixture CH_4/CO_2 were explored on a Silurian black shale sample. This outcropping sample was collected in a formation, which is not considered as target for shale gas exploration. However its geochemical profile as well as its thermal maturity suggest this sample is an ideal candidate to study kerogen/carbon dioxide and methane interactions. Both isotherm and enthalpy of adsorption of carbon dioxide were measured up to 3.2 (MPa) by the use of a combined manometric-calorimetric device. The carbon dioxide isotherm was fitted with a modified Langmuir model allowing the determination of the adsorption uptake. The heat of adsorption is an indicator of the affinity of the carbon dioxide with kerogen. Additionally the equimolar mixture methane/carbon dioxide isotherm was performed up to 2 (MPa) by use of a device specially developed and built for gas mixture co-adsorption. The adsorption of each component within the mixture was provided. The estimated selectivity CO_2/CH_4 highlights a significant affinity of CO_2 with the kerogen.

1. Introduction

The still growing demand for energy has stimulated the exploitation of unconventional gas reservoirs like shale gas. The natural gas produced from organic shale formations is known as shale gas. The total amount of natural gas is composed by three sources, i.e., the adsorbed gas, the free gas and the gas dissolved in pore fluids, the last one being negligible and consequently the total shale gas content can be considered as the sum of adsorbed and free gas (Guo, 2013; Gasparik et al., 2012). The adsorbed gas ranges from 20 to 80% of total gas reserves as well as recovery rates (Yu et al., 2014), for this reason adsorption is a leading criterion governing shale gas production. In an effort to better understand the role of adsorption on production from gas shales, numerous authors have done valuable contributions to the literature through laboratory measurements. Much research focused on the estimation of the sorption capacity of methane, the most abundant component of shale gas, at defined borehole conditions (Clarkson and Bustin, 2000; Gasparik et al., 2014a, 2014b, 2012; Guo, 2013; Mendhe et al., 2017). Most of the studies point

that methane is adsorbed onto the organic phase -known as kerogen-whereas the adsorbed gas in the inorganic matrix is generally supposed to be negligible (Collell et al., 2014; Ross and Bustin, 2009). In addition to natural gas interests, more recent studies have evaluated the potential of shales for geological CO_2 storage (Charoensuppanimit et al., 2016; Heller and Zoback, 2014). This is a remarkable observation not only for storage but also from enhanced shale gas production point of view as it implicitly points out that stronger affinity of CO_2 to the organic materials of shale could initiate an added mechanism of displacement of the originally in-place CH_4, when CO_2 is introduced into the shale gas environment. The design of the CO_2 sequestration process requires knowledge of the adsorption behavior of CO_2 (Charoensuppanimit et al., 2012). These studies showed that adsorption capacity of CO_2, as well as methane, appear to be related to the total organic carbon. Charoensuppanimit et al. (2016) focused on Woodford shales from Payne and Hancock counties. For each shale sample, CO_2 adsorption was 2.1–8.6 times higher than methane adsorption. Adsorption capacity was found correlated to the TOC content of these samples. Kang et al. (2011)

---

identified that micropores in organic matter acted as molecular sieves that allowed for only linear molecules, such as CO_2, to access their pore space. Despite these studies, gas adsorption, storage and diffusion in organic-rich shales is a complex multiparameter process that still awaits for reliable description in order to elucidate the effect of individual parameters. Indeed, kerogen is a very complex structure depending on both its origin and thermal alteration. Various realistic models have been proposed to represent the physical and chemical properties of kerogen through the use of molecular simulations (Collell et al., 2014, 2009; Sui and Yao, 2016). In the latter, Sui and Yao (2016) analysed the effect of surface chemistry for CH_4/CO_2 adsorption in kerogen. The authors proposed a 3-D molecular model of kerogen and they studied the CO_2/CH_4 interactions with kerogen. Both for pure CO_2, CH_4 or their equimolar mixture, the maximum adsorption of CO_2 in kerogen is larger than CH_4 adsorbed in kerogen. Additionally, the simulated isosteric heat of adsorption display higher values for CO_2/kerogen than for CH_4/kerogen. This is explained by the Coulomb and van der Waals interactions between CO_2 and kerogen which play a key role in the process of adsorption, whereas, in the CH_4 adsorption process, there was a little Coulomb interaction between CH_4 and kerogen.

In this context, the purpose of the present work should be regarded as a step towards the understanding of the CO_2/CH_4 interactions with kerogen. Our experimental study focused on a black shale sample outcropping in the Iberian Range from Central Spain in the province of Guadalajara. Its choice was dictate due to its basic geochemical profile and its high organic content which propose this sample as an ideal candidate to study the adsorption and interaction mechanism of both CH_4 and CO_2 with the kerogen. A complete characterization of this kerogen was performed on a previous work (Pozo et al., 2017). In the present study, sorption isotherms and heat of sorption for carbon dioxide CO_2 were measured on this selected black shale whereas the CH_4 adsorption was previously measured (Pozo et al., 2017). Additionally, the selectivity of kerogen for CH_4/CO_2 was studied from the adsorption measurement of the equimolar CH_4-CO_2 mixture at 50 °C up to 2 (MPa). To the best to our knowledge, such set of meaningful data was never presented up to the date. The experimental selectivity CO_2/CH_4 in kerogen is the main novelty of the work. Its value will provide original information to test and discriminate the realistic models proposed for the kerogen description.

The work is organized as follows. Section 2 is devoted to the description of both experimental setup and measurements principles. A fit-to-purpose calorimetric-manometric system was used to determine simultaneously adsorption isotherms and heat of adsorption of pure compounds. This apparatus can operate over broad ranges of pressure (0–3.5 MPa). The study of adsorption in gas mixture is much complicated due to the gas diffusion phenomenon. Therefore, a device was specifically designed and built for gas mixture (Pino et al., 2014) which consists of a dynamic manometric measure combined with an analytical technique. As the description of these instruments together with theirs measurement principles are extensively detailed elsewhere (Mouahid et al., 2012a, 2012b; Pino et al., 2014) we only recall theirs most significant features. In Section 3, we provide the experimental results for the pure compounds and for the equimolar mixture. The selectivity of kerogen with CO_2 and CH_4 is discussed on the basis of the results obtained for the deduced separation factor. Conclusions of this work are depicted in Section 4.

2. Experimental techniques

2.1. Sample preparation

Sorption isotherms were measured on a dry shale sample, which was received in several pieces of irregular shape; the average size of each piece was about 5 mm. Two grams of sample were dried under vacuum into the experimental cells at 110 °C during 18 h. This procedure is necessary to remove any moisture taken up by the sample. Later, after each adsorption measurement, the sample was under additional vacuum at 110 °C for 18 h, in order to withdraw any trace of fluid.

2.2. Calorimetric-manometric sorption set up

CO_2 adsorption uptake was measured using a manometric-calorimetric device. The differential heat flux calorimeter used is a Setaram C80 Tian-Calver. The inner part of the calorimeter include two calorimetric cells (reference and adsorption) surrounded by a high thermal mass aluminium block. The sample is located in the adsorption cell (see (3) in Fig. 1), which is connected to manometric apparatus inserted in the upper part of the calorimeter (Fig. 1). The same temperature is settled for the calorimeter and the manometric system allowing isothermal conditions in both parts of the coupled apparatus. The main added value of this apparatus is the simultaneous determination of the differential heat of adsorption which is a direct measurement of the adsorbate/adsorbent interactions. Note that the reference cell is used to compensate the heat flux in a blank experiment. A schematic diagram of the set-up is provided in Fig. 1.

2.3. Determination of the isotherm and heat of adsorption of CO_2

The sorption isotherms obtained by manometric measurements are excess sorption isotherms. To get more information on this concept, also called Gibbs surface excess, the reader can refer to the following work (Sircar, 1999). A mass of sample (2 gr) is placed into the adsorption cell (see (3) in Fig. 1) under vacuum. After, a quantity of gas is introduced in the dosing volume (see (2) in Fig. 1.) of known volume. The initial pressure P_1 and temperature T_1 are measured after reaching thermal and mechanical equilibria. These measurements provide the initial mole
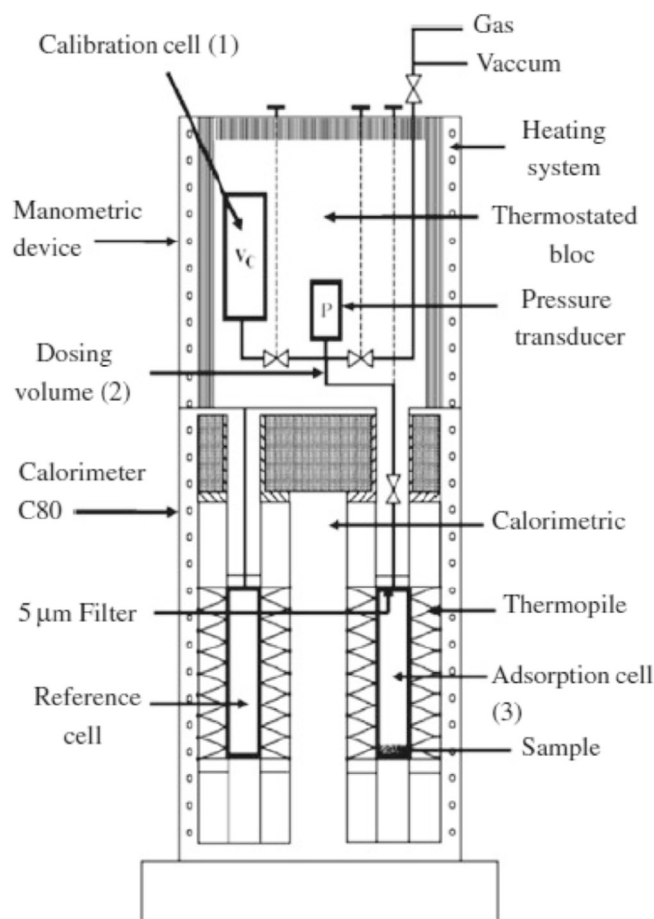

Fig. 1. Manometric-calorimetric device (Mouahid et al., 2012b).

O.P. Ortiz Cancino et al.

Journal of Petroleum Science and Engineering 159 (2017) 307–313

number of gas n_1. Then, an expansion is performed into the whole system (dosing volume and adsorption cell). As in the first step, the pressure P_2 and temperature T_2 ($T_2 = T_1$) are measured after equilibrium and the mole number remaining in the gas phase n_2 is estimated. The adsorbed mole corresponds to ($n_1 - n_2$). The isotherm is described repeating the same operations through an accumulative process. A previous measuring cell volume determination is done using Helium expansion. The molar volumes involved in the amount adsorbed calculations were determined thanks to the NIST data (Span and Wagner, 2003, 1996) at the considered experimental conditions.

2.3.1. Adsorbed amount uncertainties

After each expansion, the return to the thermodynamic equilibrium was controlled by both the pressure and calorimetric signal reached with kinetics ranging from 45 to 60 min.

The pressure is measured by a pressure transducer MKS Baratron type 121A, with an accuracy of 0.01% of the full scale (3 MPa). For temperature, the uncertainty is about 0.1 K (temperature sensor, Pt100 is located in the aluminium block of the calorimeter). The uncertainties on the dosing and measuring cell volumes have been estimated to less than 1%. The computed uncertainty on the amount adsorbed shows that the main contribution comes from the error on the pressure measurement (Belmabkhout et al., 2004). This global uncertainty is estimated to be $\frac{\Delta n}{n} = 1\%$.

2.3.2. Heat of adsorption

The heat of adsorption or differential enthalpy of adsorption ΔH (in J mol^{-1}), is also estimated at each step of the isotherm described. The calorimetric signal is representative of the total heat liberated Q, which is the result of two contributions: the heat of adsorption Q_{ads} and the heat liberated by the compressed (or expanded) gas Q_{comp}. This last contribution is previously determined through Helium expansions.

$$Q = Q_{ads} + Q_{comp} \tag{1}$$

As a consequence, the estimation of the heat of adsorption Q_{ads} requires the calculation of the heat of compression, the total heat Q being estimated through the integration of the calorimetric signal E:

$$Q = K \int E(t)dt \tag{2}$$

Expression in which K is the calorimetric detector (W·μV^{-1}), previously measured (Bessieres et al., 2005, 2000). From other part, the heat of compression Q_{comp} is determined through the use of the following Maxwell relationship:

$$\left(\frac{\partial S}{\partial p}\right)_T = -\alpha_P \cdot V \tag{3}$$

where α_P is the isobaric expansion coefficient defined by $1/V \, (\partial V/\partial T)_P$.

The heat of compression δQ_{comp} sums two contributions of opposite effect: one resulting from the gas and the other from the vessel wall:

$$\delta Q_{comp} = \alpha_{SS} V_E T dp - \alpha_p V_E T dp \tag{4}$$

In Eq. (4) α_{SS} is the isobaric coefficient of stainless steel in K^{-1} (the material of which the adsorption cell is made), T the temperature in K, and V_E is the volume taken into account by the thermopiles deduced by helium calibration:

$$V_E = \frac{k \int E(t)dt}{-(\alpha_{PHe} - \alpha_{SS})T\Delta p} \tag{5}$$

Combining Eq. (1) to Eq. (5) the heat of adsorption ΔH (J mol^{-1}) is estimated to be:

$$\Delta H = \frac{Q_{ads}}{\Delta n} = \frac{k \int E(t)dt + V_E(\alpha_P - \alpha_{SS})T\Delta p}{\Delta n} \tag{6}$$

Expression in which Δn is the amount of gas adsorbed between each step Δp.

2.3.3. Uncertainties

The procedure used to determine V_E leads to an uncertainty of $\pm 2\%$ on Q_{comp}. The error associated to the total heat Q estimated by a test of reproducibility is about 1%. Combining errors on both Q_{ads} and n_{ads}, the error on the differential enthalpy of adsorption is about 5%, strongly affected by the value of n_{ads}. The detailed procedure including both the experimental procedure and the uncertainties estimations can be found elsewhere (Bessieres et al., 2005; Mouahid et al., 2012a, 2012b).

2.4. Co-adsorption CO_2/CH_4 measurement

For the mixture, we used different pieces of the same sample. The equimolar CO_2-CH_4 mixture adsorption was measured using a device built for this purpose as is represented in Fig. 2. The principle remains identical to the pure component adsorption one (Ghoufi et al., 2009). It allows the measurements of isotherm mixture adsorption in a range of pressures from 0 to 3 MPa and for temperatures between 303.15 and 423.15 (K). A circulation pump is used to homogenize the mixture and reduces the time needed to reach equilibrium. The manometric system is coupled with a gas chromatograph (Agilent) which allows the determination of the gas mole fraction of each component in the mixture. The pressure transducer is also a MKS Baratron type 121A. To guarantee the isothermal conditions is used a heater wire controlled by a PID regulator (Eurotherm 3208); five thermocouples (type K) were installed in different parts of the circuit to ensure that there is not a temperature gradient during the measurements. This instrument has been detailed in a previous work (Pino et al., 2014).
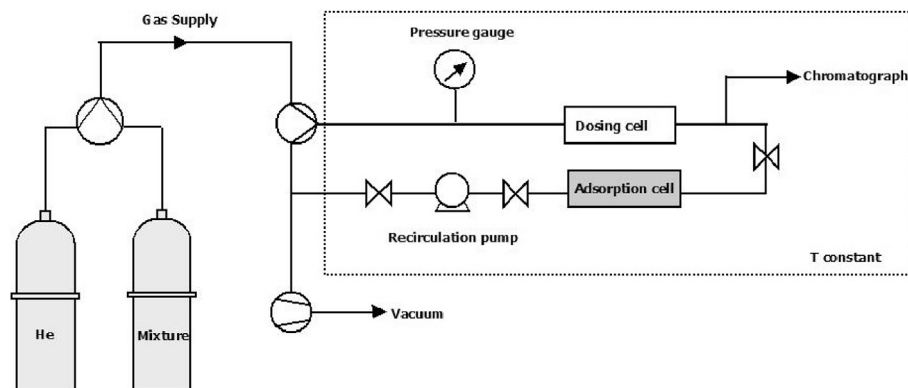

Fig. 2. Schematic diagram of the manometric dosing system.

2.4.1. Measurement principles

The procedure is analogous for pure gas. A mass of the sample (2 gr) is placed into the adsorption cell (see Fig. 2) of known volume, under vacuum. The accessible volume is determined by successive Helium expansions after what shale outgassing is carried out. Gas mixture, which is previously analysed using the chromatograph, is introduced in the dosing cell without going through the adsorption cell (see Fig. 2) until equilibrium is reached (P_1 and T_1 are measured and initial mole number of gas n_1 is calculated). In the next step, the gas expands on the whole system (dossing cell and adsorption cell, of known volumes). When both thermal, mechanical equilibria and homogenization are reached (checked by constant values of both pressure and composition) values of P_2 and T_2 ($T_2 = T_1$) are measured and the mole number remaining in gas phase n_2 is estimated. A discrete quantity of gas (0.5 cm^3) is extracted from the isolated dosing volume and analysed with the chromatograph. This measure provides the composition of the gas phase from which can be deduced the composition of the adsorbed phase. The total amount adsorbed is calculated by a mass balance (n_1-n_2). This procedure used to calculate the amounts of each individual components adsorbed was detailed in Pino et al. (2014). Basically, we wait for the equilibrium about 60 min and we perform several analyses to check reproducibility. The same operation is repeated through an accumulative process to describe the isotherm. The uncertainty on the adsorbed amount is estimated to be less than 3%.

Table 1
Characterization of black shale (CH-1).

Clay minerals (wt %)[a]	94
Non-clay minerals (wt%)[b]	6
C (wt%)	8.60
H (wt%)	1.23
N (wt%)	0.64
S (wt%)	0.09
Specific surface BET (m^2/g)	34
t-plot external surface (m^2/g)	21
t-plot micropores surface (m^2/g)	12
Micropore average size (Å)	7.6

[a] Illite (K, NH4+)-rectorite > (chlorite-kaolinite-pyrophyllite).
[b] Quartz, K-feldspar.

3. Results and discussion

3.1. Black shale sample

The shale sample named CH-1 was collected near Checa town (Guadalajara province) in the Iberian Range from Central Spain. The shale is black in color, presents lamination to slaty cleavage and contains abundant graptolite fossils dating them as Silurian (Gutiérrez-Marco and Storch, 1998). A detailed compositional analysis of this black shale including kerogen type and maturation was performed in a previous work aimed to correlate their structural and geochemical properties and the methane uptakes of different shale samples (Pozo et al., 2017). This sample consists mostly of phyllosilicates (94%) with minor contents of quartz (3%), potassium feldspar (3%) and rutile (traces) as is shown in Table 1. Within phyllosilicates predominate illite-mica and mixed-layer illite-smectite, in traces (<5%) chlorite, kaolinite and pyrophyllite were also identified (Fig. 3). The mixed-layer illite-smectite shows a high degree of ordering (R1) with sharp 001 and 002 reflections at 24.5 Å and 12.5 Å respectively, suggesting a rectorite-like clay mineral. A broad reflection was observed for illite-mica with two main maximum at 10.11 Å and 9.98 Å indicating coexistence of NH_4^+-rich illite and common illite (Daniels and Altaner, 1990). In randomly oriented samples the value of $d_{(060)}$ reflection is 1.49–1.50 Å indicating dioctahedral clay minerals.

The oriented aggregates of the clay fraction (<2 μm) corroborate the above mentioned mineralogy highlighting the swelling under ethylene glycol solvation of the regular mixed-layer illite-smectite toward 13 and 27 Å, a typical behavior of rectorite (Srodon, 1980). The identified mineralogical assemblage is similar to that previously reported in shales from the same lithological formation by Bauluz and Subías (2010). According to these authors the occurrence of NH4-rich illite and pyrophyllite result mostly from the circulation of hydrothermal fluids related to andesitic sills intruding the black shales. The content of organic carbon (TOC) reaches 8.6% and the concentration of H and N is related partially with the presence of NH_4^+ in illite interlayer (See Table 1).

3.1.1. Kerogen maturity

A Rock- Eval analysis shows that the kerogen used in this study is type III. It should be more a source of gas than oil. Here, the HI/OI ratio converges towards the origin of the plot, leading to a type III
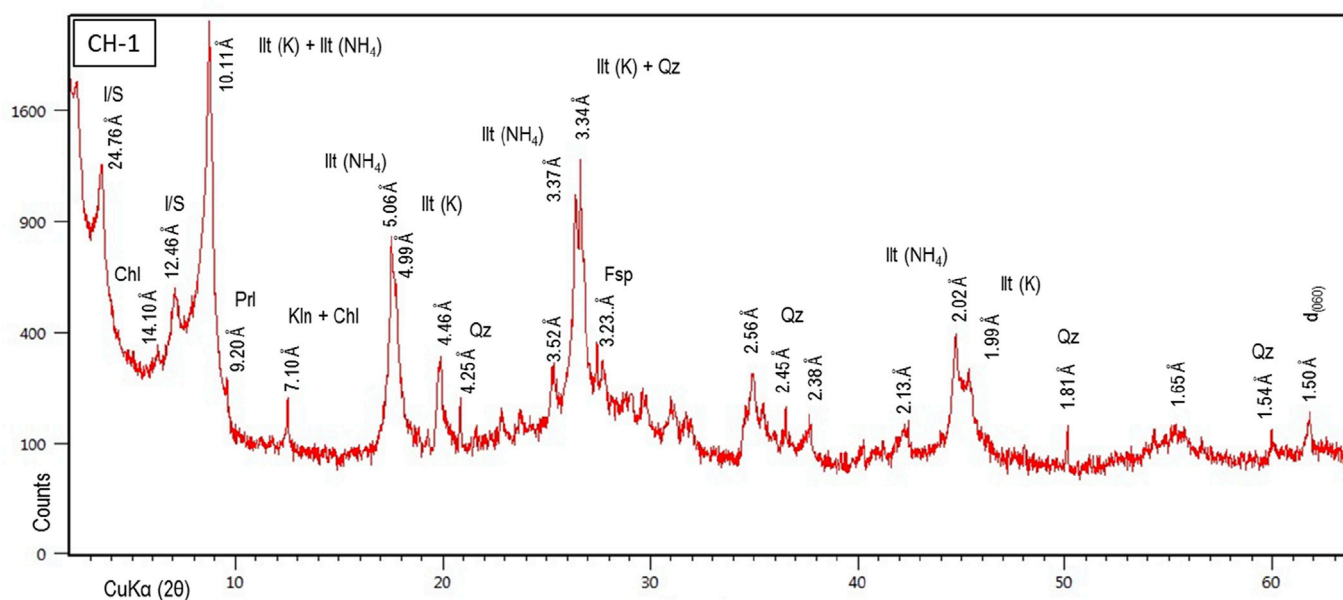

Fig. 3. X-ray diffraction pattern showing the bulk mineralogy of sample CH-1. (I/S) illite-smectite mixed layer. (Ilt) illite. (Prl) pyrophyllite. (Kln) kaolinite, (Chl) chlorite. (Qz) quartz. (Fsp) K-feldspar.

interpretation. The maturation of the sample was forced by thermal events reaching an over-mature stage. This interpretation is also supported by the very low hydrocarbon yields (S1, S2) despite their relatively high TOC content (4.4–7.62%).

The adsorption isotherm belongs to IUPAC type IV, characteristic of a wide distribution ranging from micro to mesoporous materials (2–50 nm).

CH_4 and CO_2 were provided by Linde Gas with a minimum purity of 99.995%. The equimolar mixture CH_4/CO_2 was also provided by Linde Gas. Its accuracy claimed to be better than 1% was previously checked by gas chromatograph analysis.

3.2. Pure carbon dioxide adsorption isotherm

CO_2 adsorption measurement was performed at 323K, and pressures in a range from atmospheric pressure to 3 MPa. We also reproduced the CH_4 adsorption isotherm, already studied in a previous work (Pozo et al., 2017) in which the effect of thermal events on various shales samples was depicted. Due to the limitations of the own techniques, reliable data are accessible up to moderate pressures. In this context, an alternative is to perform measurements with high accuracy up to moderate pressures (up to 3 MPa) and then fit the experimental data to a model as Langmuir, in order to obtain information to higher pressures; this procedure was followed on our work, the results are shown later. The present study focuses on CH_4/CO_2 interactions with kerogen with the idea to provide a meaningful set of data for the kerogen characterization.

Fig. 4 displays the pure CH_4 and CO_2 isotherms. These results, listed in Table 2, shows the CH_4 and CO_2 adsorption isotherms exhibit Langmuir type I behavior, which is a typical for microporous materials. This is consistent with the fact that adsorption occurs mainly onto kerogen. CO_2 adsorption is about three times larger than CH_4. At low pressures, the slope of CO_2 isotherm is higher than CH_4. This slope directly correlated to the Henry constant law (K_H) is a first indicator of the higher affinity of CO_2 with kerogen. With increasing pressure the slope decrease as the shale sample approaches saturation, in the case of methane the decrease adsorption rate is faster than CO_2 which is consistent with the higher CO_2 uptake. One can note that these values of CO_2 uptake are very similar to few values reported in the literature (Chareonsuppanimit et al., 2012; Heller and Zoback, 2014).

3.2.1. Parameterization of experimental results

To rationalize these results, the isotherm data were correlated by a Langmuir model of three parameters described by Gensterblum et al. (2009) and applied by Gasparik et al. (2012):

$$n_{ads}^{excess} = n_L \cdot \frac{p}{p + p_L}\left(1 - \frac{\rho_g(p,T)}{\rho_{ads}}\right) = n_{ads}^{absolute} \cdot \left(1 - \frac{\rho_g(p,T)}{\rho_{ads}}\right) \quad (8)$$

Expression, in which:

- n_{ads}^{excess} (mol/Kg): indicates the excess amount adsorbed at the measured pressure P (MPa).
- p_L (MPa): Langmuir pressure. The pressure at which half of the adsorption sites are occupied.
- n_L (mol/Kg): Maximum Langmuir capacity.

A standard deviation was calculated according to equation (9).

$$\Delta n = \frac{1}{N} \cdot \sqrt{\sum_1^N (n - n_{FIT})^2} \quad (9)$$

The Langmuir sorption model, developed for low pressures, represents, however, a reasonable approximation of the measured excess sorption isotherms and can thus be used as a fitting function. The main concern to apply this approach is the estimation of the maximum Langmuir capacity, which provide a value of the CO_2 adsorption capacity, in the case of this study 0.435 (mol/kg). In this work, for ρ_{ads} we used

423 kg/m^3 for methane (Gasparik et al., 2012; Pozo et al., 2017) and 1027 kg/m^3 for CO_2 (Gensterblum et al., 2013). Fitting parameters are shown in Table 3, and in Fig. 4 can be observed the isotherm obtained with these values. Note that the values obtained agree with literature values obtained for kerogen type III (Zhang et al., 2012; Gasparik et al., 2014a).

3.3. Differential heat of adsorption

The calorimetric–manometric allows a simultaneous measurement of the differential enthalpy of sorption when describing the isotherms. The values obtained for both methane (Pozo et al., 2017) and carbon dioxide are reported in Table 4. In Fig. 5, are shown the values of differential enthalpy of adsorption, ΔH_{ads}. The average value for methane reaches 30 kJ/mol whereas for carbon dioxide it is nearly 40 kJ/mol. In both cases, the values are nearly constant considering the uncertainties estimations. The behavior for CH_4 and CO_2 is consistent with physisorption because their differential heat are lower than the minimum values reported for chemisorption.

The heat of adsorption of CO_2 is larger than CH_4. This results suggest a better affinity of the CO_2 with kerogen considering that the heat or enthalpy of adsorption is directly linked to the interactions between kerogen and the species. Indeed, the enthalpy profiles nearly constant can be also regarded as the competitive effect between two opposite contributions. At low pressure the molecules are adsorbed to the high
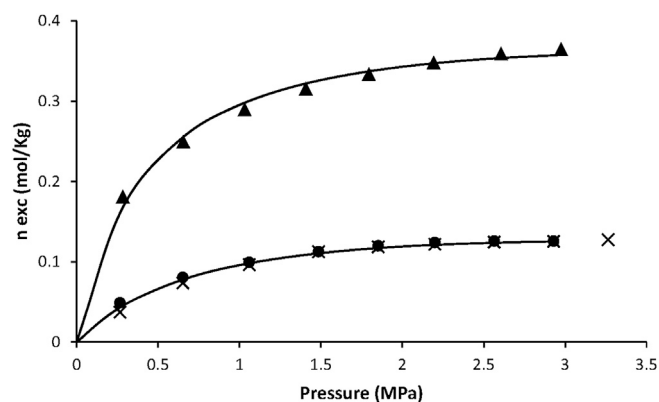

Fig. 4. Excess sorption isotherms of pure components and with fitted three parameters function (*filled circle*: CH_4 excess sorption obtained from Pozo et al., 2017, *times*: CH_4 excess sorption obtained in this work, *filled triangle*: CO_2 excess sorption, *line*: fit).

Table 2
Adsorption data for CO_2 and CH_4 pures.

CH$_4$[a]		CH$_4$ (this work)		CO$_2$	
Pressure (MPa)	n$_{exc}$(mol/Kg)	Pressure (MPa)	n$_{exc}$(mol/Kg)	Pressure (MPa)	n$_{exc}$ (mol/Kg)
0.27	0.0372	0.31	0,0478	0.28	0.1812
0.65	0.0736	0.70	0,0810	0.66	0.2499
1.06	0.0964	1.11	0,1003	1.03	0.2898
1.49	0.1124	1.57	0,1128	1.41	0.3156
1.85	0.1185	1.96	0,1191	1.79	0.3338
2.20	0.1218	2.33	0,1230	2.19	0.3480
2.57	0.1245	2.70	0,1254	2.61	0.3593
2.93	0.1254	3.07	0,1266	2.97	0.3648

[a] Pozo et al., 2017.

Table 3
Langmuir parameters with ρ_{ads} fixed.

Component	p_L (MPa)	n_L (mol/kg)	ρ_{ads} (Kg/m^3)	Δn
Methane[a]	1.00	0.222	423	0.0276
Carbon dioxide	0.45	0.435	1027	0.0025

[a] Pozo et al., 2017.

Table 4
Differential enthalpy of adsorption ΔH ads (KJ/mol).

CH_4 [a]		CH_4 (this work)		CO_2	
Pressure (MPa)	ΔH ads (KJ/mol)	Pressure (MPa)	ΔH ads (KJ/mol)	Pressure (MPa)	ΔH ads (KJ/mol)
0.10	28	0.31	25	0.28	33
0.55	35	0.70	35	1.03	44
0.90	30	1.11	28	1.41	36

[a] Pozo et al., 2017.

energy positions where as the fluid/fluid interactions play an important role when pressure is increasing. To the best of our knowledge, these differential heat of adsorption of CO_2 onto kerogen are the first experimental values reported in the literature. This meaningful information obtained on a well-characterized kerogen can be used to discriminate the different kerogen approaches proposed in the literature (Collell et al., 2014; Sui and Yao, 2016). Using a more realistic model of kerogen, molecular simulations should be performed to estimate the CH_4 or CO_2 uptakes at borehole conditions.

3.4. Equimolar mixture adsorption

Adsorption isotherm was measured for the equimolar mixture CH_4/ CO_2 in the same thermodynamics conditions that for the pure
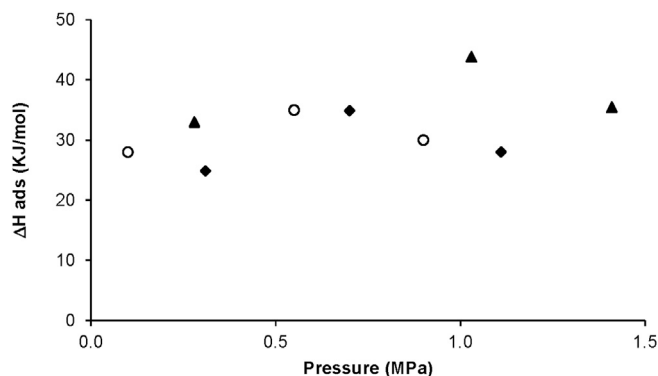

Fig. 5. Heat of Adsorption (*open circle*: CH_4 (Pozo et al., 2017), *filled diamond*: CH_4 this work, *filled triangle*: CO_2).
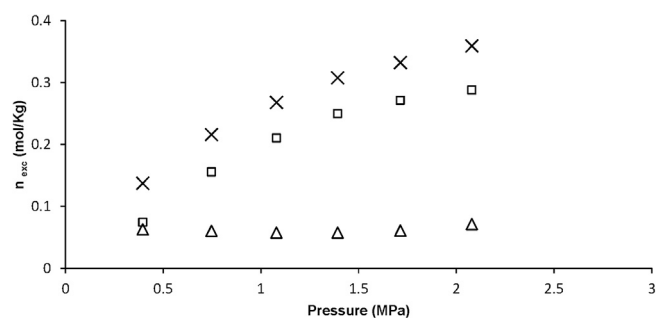

Fig. 6. Equimolar mixture sorption and individual components sorption in the mixture (*times*: mixture, *empty square*: CO_2-mixture, *empty triangle*: CH_4 mixture).

compounds. All the data are shown in Fig. 6 and summarized in Table 5. The individual gas isotherms are calculated from the mole fraction of each gas in the bulk gas phase. As expected, pure CO_2 in gas mixture is much preferentially adsorbed than CH_4. When one compare these isotherms with those of the single gas component, it is relevant that the CO_2 adsorbed amount is affected by the presence of CH_4 in the gas phase but the CH_4 amount decreases more than CO_2. All the data for the pure component in gas mixture are also summarized in Table 5. Additionally, the selectivity of CO_2 over CH_4 was calculated from equation (10) and reported in Fig. 7 as a function of pressure:

$$\text{Selectivity} = \frac{y_1/y_2}{x_1/x_2} \tag{10}$$

In this equation y is mol fraction in the bulk phase and x is mol fraction in the adsorbed phase, values are shown in Table 5. (1 for CH_4 and 2 for CO_2). This selectivity exhibits a non-monotonic evolution as a function of the pressure, with a significant increase at low pressure followed by a maximum reaching a value of 4.7 at 1.5 (MPa). This profile can be interpreted as follows: CO_2 reaches the saturation capacity whereas there is still a slight increase in CH_4 adsorption at intermediate and high pressures. A low and medium pressures, it is clearly stated that the CO_2 molecules preferentially occupy the adsorption sites. This affinity between CO_2 and kerogen is consistent both with the obtained enthalpy values and with the slope of the isotherms at very low coverage in the Henry zone.

Even if the experiment were not carried out in conditions compatible with in-well conditions, these results confirms that shale may be a promising candidate for both the gas recovery and the CO_2 storage.
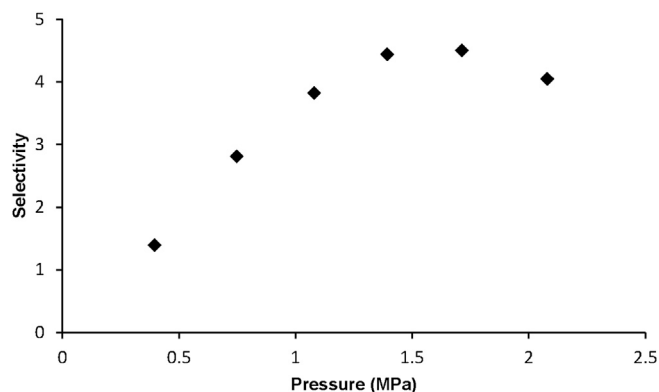

Fig. 7. Selectivity of CO_2 over CH_4 (*filled diamond:* Selectivity).

Table 5
Adsorption data for equimolar mixture and individual components in the equimolar mixture CH_4-CO_2.

Pressure (MPa)	n_{exc} mixture (mol/Kg)	n_{exc} CH_4 (mol/Kg)	n_{exc} CO_2 (mol/Kg)	y_2 CO_2	y_1 CH_4	x_2 CO_2	x_1 CH_4
0.40	0.1374	0.0630	0.0744	0.4585	0.5415	0.5415	0.4585
0.75	0.2161	0.0604	0.1557	0.4782	0.5218	0.7206	0.2794
1.08	0.2680	0.0576	0.2104	0.4885	0.5115	0.7850	0.2150
1.39	0.3077	0.0577	0.2500	0.4936	0.5064	0.8124	0.1876
1.71	0.3322	0.0609	0.2713	0.4971	0.5029	0.8167	0.1833
2.08	0.3592	0.0714	0.2878	0.4990	0.5010	0.8013	0.1987

4. Conclusions

In the present experimental study, pure and mixture adsorption properties of carbon dioxide-methane were investigated on graptolite black shale sample. This paper provides a new set of experimental data meaningful to understand of the adsorption mechanisms in shale and kerogen.

The main conclusions can be summarized as follows:

(1) Adsorption behavior of CO_2 and CH_4 exhibit type I Langmuir. CO_2 uptake is clearly greater than CH_4.
(2) Representative fits of excess sorption isotherms were obtained using a 3-parameter Langmuir-based excess sorption function. The sorption isotherms at different temperatures can be adequately represented assuming constant Langmuir sorption capacity (n_L) and sorbed phase density (ρ_{ads}) and temperature-dependent Langmuir pressure (p_L).
(3) The differential heat of adsorption is nearly constant for CO_2 and CH_4. The highest values obtained for CO_2 support the highest affinity between CO_2 and kerogen.
(4) The investigation of the equimolar mixture CO_2/CH_4 supports the higher selectivity of CO_2 over CH_4. This result is consistent with the values obtained for the differential heat of adsorption.
(5) The present works provide an original set of experimental CO_2/CH_4 selectivity in kerogen. These data are meaningful to test and discriminate the realistic model proposed for kerogen.

Acknowledgements

References

Bauluz, B., Subías, I., 2010. Coexistence of pyrophyllite, I-S, R1 and NH4+-rich illite in Silurian black shales (Sierra de Albarracín, NE Spain): metamorphic vs. hydrothermal origin. Clay Min. 45, 383–392.
Belmabkhout, Y., De Weireld, G., Frere, M., 2004. High-pressure adsorption isotherms of N2, CH4, O2 and Ar on different carbonaceous adsorbents. J. Chem. Eng. Data 49, 1379–1391.
Bessieres, D., Saint-Guirons, H., Daridon, J.L., Coxam, J.Y., 2000. Apparatus for simultaneous determination of the densities and heat capacities of liquids and of liquids with dissolved gas under an extended range of pressure (0.1-100 MPa). Meas. Sci. Technol. 11. N69.
Bessières, D., Lafitte, T., Daridon, J.-L., Randzio, S.L., 2005. High pressure thermal expansion of gases: measurements and calibration. Thermochim. Acta 428, 25–30.
Charoensuppanimit, P., Mohammad, S.A., Gasem, K.A.M., 2016. Measurements and modeling of gas adsorption on shales. Energy fuels. 30, 2309–2319.
Charoensuppanimit, P., Mohammad, S.A., Robinson, R.L., Gasem, K.A.M., 2012. High-pressure adsorption of gases on shales: measurements and modeling. Int. J. Coal Geol. 95, 34–46.
Clarkson, C.R., Bustin, R.M., 2000. Binary gas adsorption/desorption isotherms: effect of moisture and coal composition upon carbon dioxide selectivity over methane. Int. J. Coal Geol. 42, 241–271.
Collell, J., Galliero, G., Gouth, F., Montel, F., Pujol, M., Ungerer, P., Yiannourakou, M., 2014. Molecular simulation and modelisation of methane/ethane mixtures adsorption onto a microporous molecular model of kerogen under typical reservoir conditions. Microporous Mesoporous Mat. 197, 194–203.
Collell, J., Ungerer, P., Galliero, G., Yainnourakou, M., Montel, F., Pujol, M., 2009. Molecular simulation of bulk organic matter in type II shales in the middle of the oil formation window. Energy fuels. 28, 457–466.
Daniels, E.J., Altaner, S.P., 1990. Clay mineral authigenesis in coal and shale from the Anthracite region, Pennsylvania. Am. Mineral. 75, 825–839.
Gasparik, M., Bertier, P., Gensterblum, Y., Ghanizadeh, A., Krooss, B.M., Littke, R., 2014a. Geological controls on the methane storage capacity in organic-rich shales. Int. J. Coal Geol. 123, 34–51.
Gasparik, M., Ghanizadeh, A., Bertier, P., Gensterblum, Y., Bouw, S., Krooss, B.M., 2012. High-pressure methane sorption isotherms of black shales from The Netherlands. Energy fuels. 26, 4995–5004.
Gasparik, M., Rexer, T.F.T., Aplin, A.C., Billemont, P., De Weireld, G., Gensterblum, Y., Henry, M., et al., 2014b. First international inter-laboratory comparison of high-pressure CH4, CO2 and C2H6 sorption isotherms on carbonaceous shales. Int. J. Coal Geol. 132, 131–146.
Gensterblum, Y., Merkel, A., Busch, A., Krooss, B.M., 2013. High-pressure CH4 and CO2 sorption isotherms as a function of coal maturity and the influence of moisture. Int. J. Coal Geol. 118, 45–57.
Gensterblum, Y., Van Hemert, P., Billemont, P., Busch, A., Charriére, D., Li, D., Wolf, K.-H., 2009. A European inter-laboratory comparison of high pressure CO2 sorption isotherms. I: activated carbon. Carbon 47, 2958–2969.
Ghoufi, A., Gaberova, L., Rouquerol, J., Vincent, D., Llewellyn, P.L., Maurin, G., 2009. Adsorption of CO2, CH4 and their binary mixture in Faujasite NaY: a Combination of molecular simulations with gravimetry-manometry and microcalorimetry measurements. 2009. Microporous Mesoporous Mat. 119, 117–128.
Guo, S., 2013. Experimental Study on isothermal adsorption of methane gas on three shale samples from upper Paleozoic strata of the Ordos Basin. J. Pet. Sci. Eng. 110, 132–138.
Gutiérrez-Marco, J.C., Storch, P., 1998. Graptolite biostratigraphy of the lower silurian (llandovery) shelf deposits of the western iberian cordillera. Spain. Geol. Mag. 135, 71–92.
Heller, R., Zoback, M., 2014. Adsorption of methane and carbon dioxide on gas shale and pure mineral samples. J. Unconv. Oil Gas. Resour. 8, 14–24.
Kang, S.M., Fathi, E., Ambrose, R.J., Akkutlu, I.Y., Sigal, R.F., 2011. Carbon dioxide storage capacity of organic-rich shales. SPE J. 16, 842–855.
Mendhe, V.A., Mishra, S., Varma, A.K., Kamble, A.D., Bannerjee, M., Sutay, T., 2017. Gas reservoir characteristics of the lower gondwana shales in Raniganj basin of eastern India. J. Pet. Sci. Eng. 149, 649–664.
Mouahid, A., Bessieres, D., Plantier, F., Pijaudier-Cabot, G., 2012a. Supercritical adsorption of nitrogen on EcoSorb-activated carbon at temperatures up to 383 K and pressures up to 2 MPa. J. Therm. Anal. Calorim. 109, 473–479.
Mouahid, A., Bessieres, D., Plantier, F., Pijaudier-Cabot, G., 2012b. A thermostated coupled apparatus for the simultaneous determination of adsorption isotherms and differential Enthalpies of adsorption at high pressure and high temperature. J. Therm. Anal. Calorim. 109, 1077–1087.
Pino, D., Plantier, F., Bessieres, D., 2014. Experimental determination of the adsorption isotherms in gas mixtures under extended pressure and temperature range: application to the CO2–CH4 binary mixture. J. Therm. Anal. Calorim. 117, 1469–1477.
Pozo, M., Pino, D., Bessieres, D., 2017. Effect of thermal events on maturation and methane adsorption of ammonium illite-rich Silurian black shales (Checa, Spain). Appl. Clay Sci. 136, 208–218.
Ross, D., Bustin, R.M., 2009. The importance of shale composition and pore structure upon gas storage potential of shale gas reservoirs. Mar. Pet. Geol. 26, 916–927.
Sircar, S., 1999. Gibbsin surface excess for gas adsorption8 Gibbsian surface excess for gas adsorption. Ind. Eng. Chem. Res. 28, 3670–3682.
Span, R., Wagner, W., 1996. 1996. A new equations of state for carbon dioxide covering the fluid region from the triple point temperature to 1100 K at pressures up to 800 MPa. J. Phys. Chem. Ref. Data 25 (6), 1509–1596.
Span, R., Wagner, W., 2003. Equations of State for Technical Applications. I. Simultaneously optimized functional Forms for nonpolar and polar fluids. Int. J. Thermophys. 24, 1–39.
Srodon, J., 1980. Precise identification of illite/smectite interstratifications by X-ray powder diffraction. Clays Clay Min. 28, 401–411.
Sui, H., Yao, J., 2016. Effect of surface chemistry for CH4/CO2 adsorption in kerogen: a molecular simulation study. J. Nat. Gas. Sci. Eng. 31, 738–746.
Yu, S., Chen, H., Yang, S., Guo, X., Zhou, Ch, Fang, B., Zhou, F., Yang, J.K., 2014. A new mathematical model considering adsorption and desorption process for productivity prediction of volume fractured horizontal wells in shale gas reservoirs. J. Nat. Gas. Sci. Eng. 19, 228–236.
Zhang, T., Ellis, G.S., Rupple, S.C., Milliken, K., Yang, R., 2012. Effect of organic matter type and thermal maturity on methane adsorption in shale-gas systems. Org. Geochem. 47, 120–131.